Contrasted electronic properties of Sn-adatom-based (3 x 3) R 30 ° reconstructions on Si(111)

Anne Charrier, R. Pérez, F. Thibaudau, J.-M. Debever, J. Ortega, F. Flores, Jean-Marc Themlin

Contrasted electronic properties of Sn-adatom-based $(\sqrt{3}\times\sqrt{3})R30°$ reconstructions on Si(111)

A. Charrier,[1,*] R. Pérez,[2] F. Thibaudau,[1] J.-M. Debever,[1] J. Ortega,[2] F. Flores,[2] and J.-M. Themlin[1]
[1]*Groupe de Physique des Etats Condensés, Faculté des Sciences de Luminy, Université de la Méditerranée, Case 901, 13288 Marseille Cedex 9, France*
[2]*Departamento de Física Teórica de la Materia Condensada, Facultad de Ciencias, Universidad Autónoma de Madrid, Madrid 28049, Spain*

(Received 17 January 2001; revised manuscript received 6 April 2001; published 23 August 2001)

We have investigated the electronic structure of the two-dimensional solid solution $Si_xSn_{1-x}/Si(111)$-$(\sqrt{3}\times\sqrt{3})R30°$ at room temperature, with a particular emphasis on the empty states, using both global [$k_{//}$-resolved inverse photoemission spectroscopy (KRIPES)] and local probes (scanning tunneling microscopy and spectroscopy, STM and STS), as well as DFT-LDA calculations. This adatom overlayer with a $(\sqrt{3}\times\sqrt{3})R30°$ symmetry shows drastic evolution with increasing Sn-adatom concentration, including a semiconductor to metal transition. The $Si_{0.5}Sn_{0.5}/Si(111)$-$\sqrt{3}$ or mosaic phase has a single empty surface state localized at 0.56 eV above E_F at $\bar{\Gamma}$. With an overall bandwidth of ≈ 0.15 eV, this sp_z-type state localized on Si adatoms does not cross E_F: the mosaic phase is semiconducting, with a bandgap between 0.3 and 0.5 eV. This phase is characterized by a large corrugation of 0.75 Å with Sn adatoms higher than Si adatoms. In the Sn-rich limit $Si_xSn_{1-x}/Si(111)$-$\sqrt{3}$ with $x \leqslant 0.05$, we follow an empty state U_1' throughout most of the surface Brillouin zone except near the $\bar{K}$ point where it clearly crosses the Fermi level. A second, empty surface state U_2' is detected 1.67 eV above E_F. Once correlation effects suggested by the small bandwidth of U_1' are adequately taken into account, we explain our KRIPES results in the framework of a dynamical fluctuations model as originating from an underlying (3×3) structure. Finally, results pertaining to intermediate Sn-adatom concentrations are interpreted in view of the two limiting cases.

DOI: 10.1103/PhysRevB.64.115407 PACS number(s): 73.20.At, 71.30.+h, 71.27.+a, 79.60.Jv

I. INTRODUCTION

Adsorption of submonolayer amounts of Sn on Si(111) induces a wealth of reconstructions.[1] Among these, the $(\sqrt{3}\times\sqrt{3})R30°$ reconstruction (hereafter called $\sqrt{3}$ for brevity), an old and familiar object in surface science, consists of a low-density adatom overlayer on top of a bulk-truncated Si(111),[2] which can be stabilized at room temperature for a broad Sn coverage continuously varying between 1/6 and 1/3 ML.[3] The widely accepted description of this overlayer involves 1/3 ML of adatoms located at T_4 sites,[4] forming an hexagonal array with the $\sqrt{3}$ symmetry, with one adatom per $\sqrt{3}$ unit cell.[5] These threefold-coordinated adatoms are located at T_4 sites directly above second layer substrate atoms and are bound to three atoms of the substrate first layer. However, each T_4 site can accommodate either a Sn or a Si adatom. Depending on the initial Sn coverage and annealing temperature, the overlayer can thus accommodate a wide range of compositions, and is best viewed as a purely 2D solid solution $Si_xSn_{1-x}/Si(111)$-$\sqrt{3}$[6], where a fraction ($x \leqslant 0.5$) of the Sn adatoms may be substituted by isovalent Si adatoms. Historically, the two limiting cases corresponding to $x=0$ (100% Sn) and $x=0.5$ have been called the $\alpha-\sqrt{3}$ and $\gamma-\sqrt{3}$ (or mosaic) phases.[7] In what follows, and although it is understood that they are just the limiting cases of a single phase, we will be using the notation $\alpha-\sqrt{3}$ and $\gamma-\sqrt{3}$ and we will refer to these particular cases as if they were distinct phases. Furthermore, it should also be stressed that the ideal $Si_xSn_{1-x}/Si(111)$-$\sqrt{3}$ ($x=0$) cannot be prepared at room temperature since a number of Si substitutional defects is always present: x has therefore a lower practical bound of the order of 0.03.

As far as the electronic structure is concerned, with a single tetravalent adatom per unit cell, it would be expected that the $\sqrt{3}$ reconstruction keeps a metallic character for all Sn coverages, since three electrons are involved in the covalent bonding with the substrate and one electron remains in the Sn or Si adatom dangling bond. On the basis of simple electron counting rules, we expect a single metallic surface state crossing E_F, derived from the sp_z-like orbitals localized on each adatom.[8] However, this is far to be the case for the $\gamma-\sqrt{3}$, obtained at a coverage of 1/6 ML of Sn (x=0.5).[9] The $\gamma-\sqrt{3}$, also called mosaic phase and its characteristic kinked lines were first discovered on the Sn/Si(111)-$\sqrt{3}$ interface[10,11] and then observed on the Pb/Si(111) system.[12] On Pb/Si(111)-$\sqrt{3}$, Karlsson *et al.*[13] have evidenced a charge transfer from Si adatoms to Pb adatoms. Later, scanning tunneling microscopy (STM) measurements[9,14] revealed the same behavior for Sn/Si. Such a charge transfer induces the presence of two surface states, above and below the Fermi level, and the surface is semiconducting. However, the experimental and theoretical evidence reporting the existence, position, overall bandwidth and dispersion of these states is still scarce, especially for the unoccupied states. Early angle-resolved photoemission[15] and inverse photoemission[16,17] on Sn/Si(111)-$\sqrt{3}$ which do show two distinct states and no obvious Fermi level crossing concluded however to a metallic character. Furthermore, the latter results being anterior to the first report of the mosaic phase, it is not clear on which type of $\sqrt{3}$ the experiments applied, either the mosaic, the alpha phase or an intermediate. We

have measured the unoccupied state of the mosaic phase and its detailed dispersion using $k_{//}$-resolved inverse photoemission spectroscopy. As expected, this state does not cross the Fermi level, and scanning tunneling spectroscopy (STS) measurements confirm that the surface is semiconducting, in good agreement with our theoretical calculations.

As additional Sn adatoms are added to the overlayer, $Si_xSn_{1-x}/Si(111)$-$\sqrt{3}$ ($x<0.5$) should undergo a semiconductor to metal transition, since the host ($x\approx 0$) $\alpha-\sqrt{3}$ phase, which can be stabilized at room temperature, only contains Sn adatoms (at a coverage of 1/3 ML). The availability of a single site clearly prevents any charge transfer, and the reconstruction, at first sight, should be metallic. However, we are still missing a clear spectroscopic evidence of the Fermi level crossing for $\alpha-\sqrt{3}$. We will show that most of this ''metallic'' sp_z-adatom derived state is indeed unoccupied and can be followed in a large portion of the reconstructed surface Brillouin zone (SBZ). The Fermi level crossing is clearly visible in the immediate vicinity of the $\overline{K}$ point, where the state disappears from the angle-resolved KRIPES spectra. The overall bandwidth of this state is small, of the order of 0.55 eV, so correlation effects are expected to play a role.

There are, however, some additional puzzling results. While the above-described picture of the $\alpha-\sqrt{3}$ phase readily accounts for a single metallic surface state, we have observed a second empty surface state 1.67 eV above the Fermi level. This observation is not compatible with the existence of a single T_4 site, but rather suggests that more than one site is involved in the actual structure of the $\alpha-\sqrt{3}$ phase. This has already been suggested by previous photoemission studies[18] which have shown that the Sn $4d$ core level intriguingly contains two components. Similar results have been observed for the closely related Sn/Ge(111) system.[19,20] In this case, the room-temperature (RT) $\alpha-\sqrt{3}$ phase undergoes a structural phase transition at low temperature to a 3×3 phase.[21] On the basis of first-principles molecular dynamics simulations, this transition has been interpreted[19] in terms of a dynamical fluctuations model in which fluctuating adatoms at room temperature, are stabilized in a 3×3 phase at low temperatures. Surface x-ray diffraction studies[22,23] and DFT-LDA calculations[19,24] show that the low temperature phase is a 3×3 reconstruction with two different types of Sn adatoms, both on T_4 sites, but one ~ 0.3 Å higher than the other. This low-temperature phase has also been proposed to correspond to the formation of a charge density wave.[21] Some recent results indicate that Sn/Si(111) should also exhibit such atomic fluctuations,[25] although no 3×3 phase is expected to appear at low temperature.[26,27] Based on this fluctuations model, our KRIPES data receive a natural explanation provided that correlation effects are properly taken into account. Finally, results pertaining to intermediate phases are interpreted in view of the two limiting cases.

II. EXPERIMENTAL PROCEDURES

KRIPES experiments were performed in an ultrahigh-vacuum chamber (base pressure 3×10^{-10} mbar) equipped with a low-energy electron diffractometer (LEED) and an inverse photoemission setup.[28] The latter consists of an electron gun and an elliptical mirror to focus photons emitted in a large solid angle towards the photon detector. The Geiger-Müller type detector filled with a helium-iodine mixture and sealed with a SrF_2 window operates in an isochromat mode at a fixed photon energy of 9.5 eV. The overall energy resolution, determined by measuring the Fermi edge on a Ta foil, is 0.35 eV, including the electron gun and the detector. The dispersion within the surface Brillouin zone (SBZ) of interest is investigated by rotating the electron gun in a vertical plane perpendicular to the sample surface (variable polar angle with respect to the surface normal) and oriented along a given azimuth.

STM and STS experiments were performed in an ultrahigh vacuum chamber equipped with an OMICRON system (base pressure 1×10^{-10} mbar) and a tungsten tip. The typical setpoint current used to obtain STM images and STS measurements were, respectively, 50 and 100 pA. STS results represent an average over the surface obtained with 47 measurements, each of them being taken with an acquisition time of 50 ms.

We used phosphorus-doped (resistivity $\sim 2\times10^{-2}$ Ω cm) Si(111) wafer samples of size $20\times5\times0.28$ mm^3. Before introducing into vacuum, the sample is chemically prepared *ex situ* by a wet hydrogenation procedure. In the KRIPES setup, the sample is then annealed in UHV by electron bombardment on its reverse side using a BaO cathode. In the STM case, annealing is performed by direct Joule heating. The annealing temperature was monitored by an infrared pyrometer assuming an emissivity of 0.8.[29] The starting point before evaporation of Sn was the 7×7 reconstruction obtained by annealing the Si sample around 1200°C. $\sqrt{3}$ phases are obtained by the deposition of approximately 1.5 ML of Sn at RT. The surface is then annealed at 630 °C during 2 min for the $\alpha-\sqrt{3}$ phase, 4 minutes for the $\gamma-\sqrt{3}$ phase, and between 2 and 4 minutes for the intermediate phases. The orientation and surface quality of every surface reconstruction was checked by LEED.

III. STM RESULTS

One of the most difficult part of this work was the preparation of the appropriate surface, since markedly different reconstructions with very similar $\sqrt{3}\times\sqrt{3}$ symmetry and the same diffraction pattern may be prepared for the Sn/Si(111) interface. Within the adatom layer, a continuum of Sn adatom concentrations can be obtained between two limits of 1/6 ML (the γ or mosaic phase) and 1/3 ML of Sn (the α phase).

In order to calibrate our preparation procedure and to understand the differences between these phases, we have realized a scanning tunneling microscopy study for both α and γ phases as well as for intermediate cases. Figures 1(a)–1(f) shows STM images of three phases. Images (a) and (b) were obtained on the mosaic phase at, respectively, -1 V (occu-

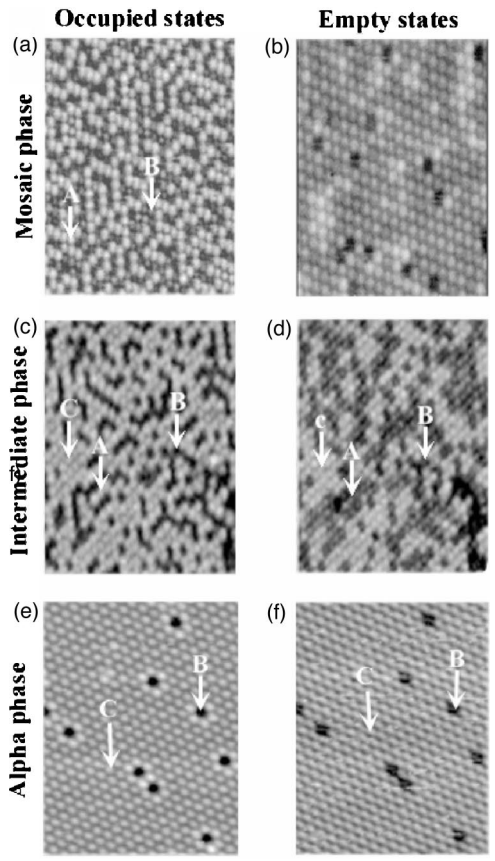

FIG. 1. STM images obtained on three phases of $Si_xSn_{1-x}/Si(111)-\sqrt{3}$. (a) and (b) show images of the mosaic phase ($x \simeq 0.5$) respectively obtained at -1 V (occupied states) and 1 V (empty states). (c) and (d) represent the intermediate phase at -0.45 V and 0.45 V. (e) and (f) are images of the α phase ($x \simeq 0$) at -0.45 and 0.45 V. Images of the intermediate and alpha phases have been taken simultaneously at the same location.

pied states) and 1 V (empty states); (c) and (d) represent an intermediate phase at -0.45 and 0.45 V and finally (e) and (f) are images obtained on the α phase at -0.45 and 0.45 V. The three sets of images obtained for each phase are very different. Three types of adatom sites can be observed on this image as indicated in Table I.

The mosaic phase [Figs. 1(a) and 1(b)] is known to contain an equal amount of Sn and Si adatoms.[9] The possibility of a charge transfer between Sn and Si adatoms is neglected in a first approach; they are both tetravalent and share the same electronegativity. Since all the adatoms are bound to

TABLE I. Different types of adatom sites observed on the mosaic, intermediate, and α phases.

	Mosaic		Intermediate		Alpha	
	Occupied	Empty	Occupied	Empty	Occupied	Empty
Type A	Bright	Dark	Bright	Dark		
Type B	Dark	Dark	Dark	Dark	Dark	Dark
type C			Bright	Bright	Bright	Bright

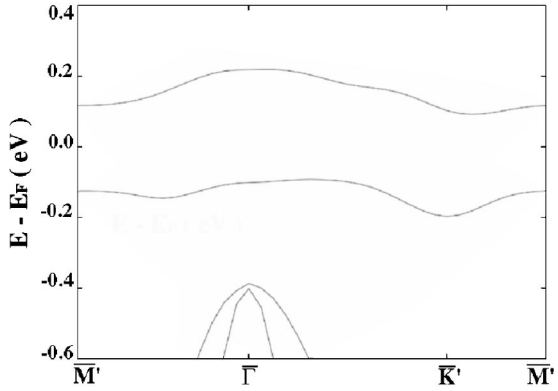

FIG. 2. Surface band structure along the symmetry directions M'-Γ-K'-M' of the SBZ for Sn/Si(111)$-(2\sqrt{3}\times\sqrt{3})$ with one Sn adatom and one Si adatom, simulating the mosaic structure. The lower (occupied) surface band is associated with the Sn dangling bond while the upper (empty) surface band is related to the Si dangling bond. The energy of these bands is indicated with respect to the Fermi level. The surface is semiconducting.

three atoms of the outermost Si layer, their dangling bond should hold one electron. The density of occupied and empty states observed in the STM images is thus expected to be quite homogeneous over the surface. Although this is the case in the empty states,[30] two types of protrusions (A and B) are seen in the occupied states [Fig. 1(a)]. An estimation of the amount of the protrusions for these two families indicates the presence of about 50% of each. Each family of protrusions must correspond to either Sn or Si adatoms.

Can we explain this large intensity difference on the sole basis of structural arguments? The covalent radius of Sn (1.40 Å) is larger than that of Si (1.17 Å), but a cross section of the occupied state indicates a corrugation of 1.6 Å, much larger than the covalent radii difference. This implies that we can expect an important topographic corrugation with the tin atoms in a position higher than that of Si.

We have analyzed the adatom geometry corresponding to the mosaic phase, using a first-principles DFT-LDA tight-binding molecular dynamics technique.[31] In these calculations we have assumed, for the sake of simplicity, a $2\sqrt{3}\times\sqrt{3}$ geometry with one Sn adatom and one Si adatom per surface unit cell. Four Si layers are included in the calculation, and the lower one is saturated by H atoms. We find that, once the atomic positions are relaxed to their minimum energy configuration, the Sn adatoms are higher than Si adatoms by ~ 0.75 Å. The total corrugation seen in STM, i.e., 1.6 Å, is larger than this physical corrugation plus the difference of the covalent atomic radii (~ 0.23 Å): this can be ascribed to the electron charge transfer from Si to Sn associated with the formation of a semiconductor gap at E_F. Figure 2 shows the electronic band structure for this surface [$Si_{0.5}Sn_{0.5}/Si(111)$-$2\sqrt{3}\times\sqrt{3}$]. Our calculations show an energy gap of 0.25 eV between Sn-like filled states and Si-like empty states.

As the amount of tin is slightly increased, intermediate phases can be observed, such as the one shown in Figs. 1(c) and 1(d). In addition to the *A*- and *B*-type protrusions of the mosaic phase, we observe a *C*-type adatom site and the total

number of white protrusions is increased in both occupied and empty states with respect to the mosaic phase. In the occupied states, these white protrusions must thus correspond to Sn adatoms and the charge transfer occurs from Si adatom towards Sn adatom,[7] in agreement with the LDA calculations mentioned above. This charge transfer perfectly explains the mosaic images; the large difference in density of states is accentuated at -1 V and compensated at 1V (in terms of intensity) by the difference in heights between Sn and Si adatoms.

In the intermediate phase, this charge transfer cannot involve all the Sn adatoms since there are more Sn than Si adatoms. That makes the difference between *A* and *C* types of Sn adatoms. The *A*-type adatoms still make the charge transfer and have a fully occupied DB while the *C*-type Sn adatoms remain with a half-filled DB. The latter appear white in both occupied and empty states (we will see below that these half-filled DB have to be understood as the average of the DB occupancies associated with height-fluctuating adatoms). The dark protrusions in the empty states are attributed to Si (*B*-type) and *A*-type Sn adatoms. The reason why the Si adatoms with empty DBs appear dark is related to their location (~ 0.5 Å below the Sn adatoms with half-occupied DBs) which reduces the Si adatom contribution to the STM image.

The α phase [Figs. 1(e) and 1(f)] mainly contains *C*-type Sn adatoms ($\geqslant 97\%$) and a few defects ($\leqslant 3\%$ of substitutional Si adatoms, *B* type). The brightest protrusions around the defects have recently been interpreted in terms of a localized 3×3 periodicity stabilized around the defects at RT.[26]

IV. THE α-$\sqrt{3}$ PHASE

Figures 3(a) and 3(b) shows KRIPES results measured on the α phase. These spectra were obtained along the two high-symmetry directions $\overline{\Gamma K'}$ and $\overline{\Gamma M'}$ of the reconstructed surface Brillouin zone, for various polar angles of the incident electron beam on one side of the surface normal for each azimuth. These spectra give the number of detected photons (normalized to the incident current on the sample) versus the electron energy with respect to the Fermi level (E_F). In order to find the positions of the different empty states, a background line is removed from the raw data (dots) and the spectra is then fitted with a set of Gaussians. The final fit is given by a continuous line. The maximum of each Gaussian, marked by a vertical bar, indicates the presence of an empty state. A set of five Gaussians was necessary to fit the spectra, indicating the presence of five different states. In both directions $\overline{\Gamma K'}$ and $\overline{\Gamma M'}$, the intensity of the first two states is maximum at normal incidence (the SBZ center is probed) and decreases as the angle of incidence of the electrons increases (the SBZ edge is probed) while the intensity of the upper states remains almost unchanged for every angle. All these states can be followed along the $\overline{\Gamma M'}$ direction, and therefore do not cross E_F along this azimuth. Along the $\overline{\Gamma K'}$ direction, the four upper states are followed all over the SBZ whereas the lower one approaches E_F as the polar angle increases and finally disappers around 30° ($k_{//}\simeq 0.6$ Å^{-1}).

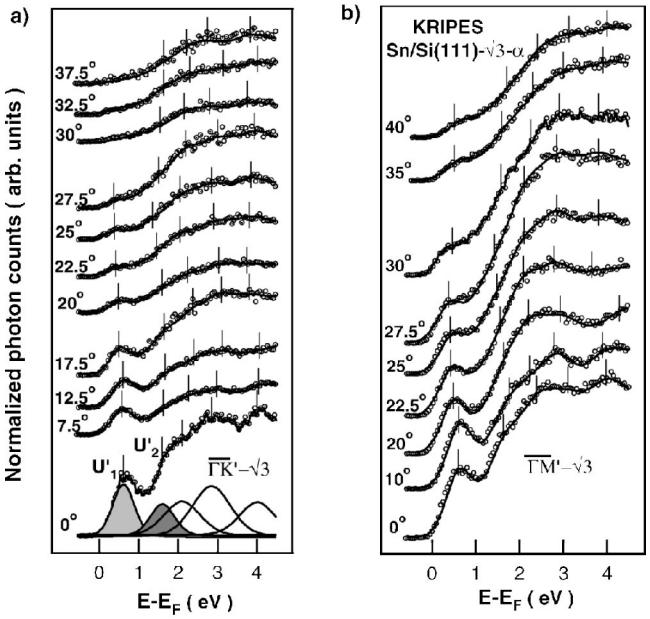

FIG. 3. KRIPES spectra of the $\alpha-\sqrt{3}$ surface along the $\overline{\Gamma K'}$ (a) and $\overline{\Gamma M'}$ (b) directions of the SBZ for selected angles of the incident electrons. Experimental curves are plotted as circles, the fit is represented by a continuous line, and each Gaussian maximum is marked by a vertical bar.

This Fermi level crossing gives a metallic character to the surface.

This metallic nature has been confirmed by scanning tunneling spectroscopy (STS) [Fig. 4(a)]; this spectrum gives the current intensity crossing the surface versus the voltage applied to the tip. The current-voltage characteristic is linear at these low voltages, a typical result for STS of metals. This STS curve has not been taken over a single adatom site but rather represents the average behavior of the surface.

The determination of the origin of the observed states requires further experiments, since each state can be interpreted as surface states, surface resonances or bulk states. A simple experiment consists in saturating the dangling bonds without modifying the surface reconstruction by exposure to atomic hydrogen, obtained through dissociation of the molecule by a nearby hot filament. Figure 5 shows spectra of the α phase under the same conditions (a) before and (b) after exposure at $\overline{\Gamma}$. After exposure, the intensity decrease mainly

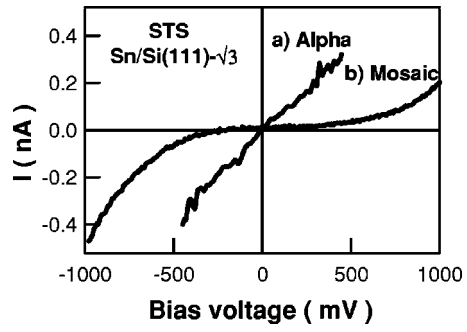

FIG. 4. STS measurements of the α (a) and mosaic (b) phases. We used a typical setpoint of 100 pA and the spectra represent an average over the surface obtained from 47 measurements.

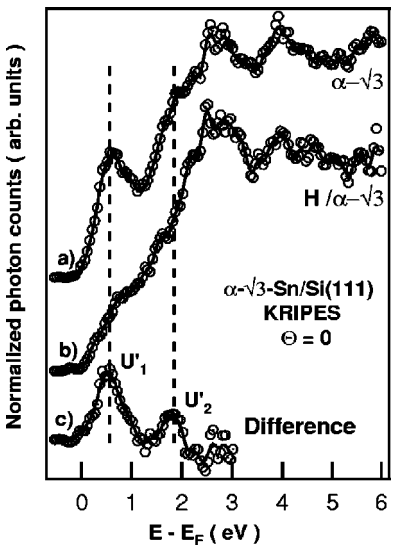

FIG. 5. (a) and (b) KRIPES spectra of the α phase respectively obtained before and after exposure of the sample to 1L of atomic hydrogen. (c) Difference curve (a),(b).

concerns U_1' and U_2'. This decrease is emphasized in spectrum (c), the difference between the two previous spectra which reveals the adsorption-sensitive surface states (the reversibility of this procedure by heating indicates the conservation of the surface reconstruction during hydrogenation). The higher three energy states which remain unaffected by the hydrogen are interpreted as bulk states. The surface states U_1' and U_2' are, respectively, found at 0.58 and 1.67 eV above E_F at $\bar{\Gamma}$.

Figure 6 shows the band dispersion of the different states, i.e., the electron energy versus the wave-vector projected parallel to the surface. Results obtained with positive and negative angles, i.e., from both sides of surface normal for a given azimuth have been superimposed. The shape of the

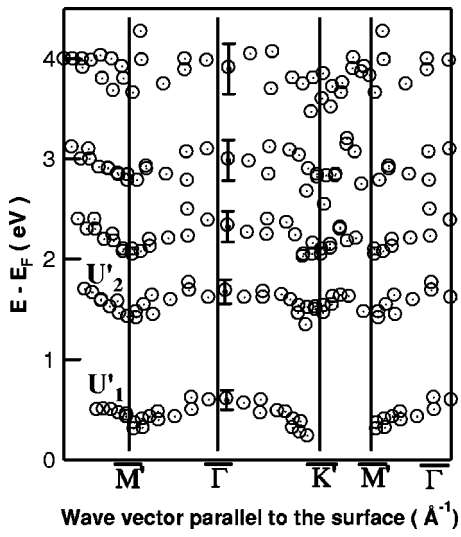

FIG. 6. Unoccupied band dispersions $E(k_{//})$ of the α phase. Electron energy is plotted against the wave vector parallel to the surface.

band dispersions of U_1' and U_2', which shift towards E_F when approaching the SBZ edges is characteristic of a p_z adatom derived surface state.[8,32] Moreover, Nicholls *et al.*[33] have shown that for adatoms in T_4 sites, substrate atom orbitals with wave vectors near the edges of the 1×1 SBZ couple favorably to the adatom states, giving rise to an occupied state, while those with wave vector near the 1×1 SBZ center give rise to empty states. Thus, in the empty states, we expect a high intensity near $\bar{\Gamma}$ which decreases as we approach the SBZ edges. Although our KRIPES spectra have been taken up to 40° only, the behavior of the intensity of the first peak is in good agreement with this theory (the 1×1 SBZ edge corresponds to about 50°). We thus conclude that U_1' and U_2' are adatom-derived surface states. Moreover, since the α-$\sqrt{3}$ phase contains more than 97% of Sn adatoms, both of these states are characteristic of Sn. We also notice that their band dispersions are similar, although the bandwidth of U_2' ($W_2=0.4$ eV) is smaller than that of U_1' ($W_1\geqslant0.58$ eV).

The α-$\sqrt{3}$ reconstruction is usually described with a single Sn adatom per unit cell, with one electron per adatom dangling bond. This model is seriously questioned by the existence of two empty surface states U_1' and U_2', a result that suggests the presence of more than one type of adatom in this surface. The existence of at least two types of adatom sites for this phase has also been suggested by Sn $4d$ core level measurements[18,34,35] which reveal the presence of at least two components.

Similar results have been observed on the Sn/Ge(111) interface[19,20] across the reversible $\sqrt{3}\times\sqrt{3}R30°\leftrightarrow3\times3$ phase transition using core level and valence-band photoemission spectroscopies. They found, both below and above the transition, two components in the Sn $4d$ core level and two occupied surface states, one of them crossing the Fermi level. Theoretical calculations[19,24] show that these two effects are due to the existence of two structurally different types of Sn adatoms in the ground state of the system (the 3×3 reconstruction), both on T_4 sites but one ~0.3 Å higher than the other. The ''up'' adatoms present fully occupied DBs (occupancy = 1) while the remaining electron (per 3×3 unit cell) is shared by two ''down'' DBs (occupancy = 1/4).[24] It has been recently shown that the $\sqrt{3}\times\sqrt{3}\leftrightarrow3\times3$ phase transition in Sn/Ge(111) is associated with a surface soft phonon[27] where the Sn adatoms display at RT correlated up/down vibrations with large amplitudes, keeping memory of the underlying 3×3 phase. These dynamical fluctuations[19] explain the two components in the Sn $4d$ core level and the two occupied surface states observed for the α-$\sqrt{3}$ phase.

The Sn/Si(111) system does not display the $\alpha-\sqrt{3}\leftrightarrow3\times3$ transition,[26] since the $\sqrt{3}$ is the stable structure at low T.[27] Nevertheless, the atomic motion at RT is similar to the Sn/Ge case, since the vibration associated with the 3×3 structure is a minimum of the surface phonon dispersion and the atomic motion should be dominated by this mode.[27] In other words, the soft phonon responsible for the $\alpha-\sqrt{3}\leftrightarrow3\times3$ transition in Sn/Ge is partially softened in the Sn/Si case, explaining the similarities of both cases at RT; in particular, the Sn/Si(111)-α-$\sqrt{3}$ electronic structure is also determined

by locally fluctuating "3×3" atomic geometries.

In order to understand the electronic properties of the Sn/Si(111)-α-$\sqrt{3}$ surface, and in particular its unoccupied surface bands, we have to analyze the electronic structure of the underlying 3×3 geometries. At RT the Sn adatoms vibrate between "up" and "down" positions (see Ref. 27) which differ by $\Delta z\sim0.3$ Å ; thus, the electronic structure of a Sn/Si(111)-3×3 surface, with $\Delta z\sim0.3$ Å has been analyzed.[36] The LDA result shows a fully occupied surface band ~0.15 eV below E_F, and two overlapping surface bands at E_F with a bandwidth of $W\sim0.3$ eV and an occupancy of 1/4 (i.e., one electron for two bands). The effective intrasite coulomb interaction U_{eff} for the Sn-dangling bonds is estimated to be $U_{\text{eff}}=1.15$ eV,[36] i.e., $U_{\text{eff}}\gg W$ and electron correlation effects have to be considered. Figure 7(a) schematically shows how the LDA band at E_F is changed when introducing electron correlations: the effect of U_{eff} is to create a new state at E_F+U_{eff}, with 1/4th of the initial weight, while the weight of the state that remains at E_F is reduced by 3/4 (i.e., three electrons per 3×3 unit cell).

This theoretical analysis, including many-body effects, is in very good agreement with the experimental KRIPES results: the band at E_F is identified with U_1', while the band at E_F+U_{eff} perfectly explains the U_2' state. Moreover, the difference in energy of the two empty surface states, 1.1 eV, is very close to the theoretical result $U_{\text{eff}}=1.15$ eV. This good agreement between experimental and theoretical results for the unoccupied surface bands provides a strong support to the interpretation of the Sn/Si(111)-α-$\sqrt{3}$ surface as a dynamically fluctuating phase in which, at RT, the atomic motion is dominated by a 3×3 surface phonon.[27] In Sec. VI, an independent confirmation of the weight of U_1' will support the present interpretation further. We also mention that if the Sn adatoms are assumed to be at the same height on the surface, one would expect for the surface electronic structure a Mott-Hubbard transition as in the case of SiC-$\sqrt{3}$ (Ref. 32) and the surface should be semiconducting [see Fig. 7(b)], in disagreement with the experimental evidence.

It should be mentioned that this interpretation of the α-$\sqrt{3}$ phase is not incompatible with the relative flatness of the STM images on the α phase [Figs. 1(e),1(f)], although the weak corrugation on these images suggests the presence of a single type of adatom site. In this model where the adatoms fluctuate, the STM acquisition time is far too slow to see these adatom fluctuations. What we observe is an average of these two adatom positions [the Sn half-filled DB of Figs. 1(c),1(d) can also be associated with this fluctuations model].

Conway *et al.* using x-ray diffraction experiments and Keating strain energy minimization have determined a single value of 1.58 Å for the Sn adatom height on Sn/Si(111)-$\sqrt{3}\times\sqrt{3}$.[37] Apart from the fact that the detailed stoichiometry in the adatom layer is unknown in this early experiment, this value is not compatible with a mean value of more than 2 Å obtained from electron standing waves recently reported by Yamanaka and Ino, who have questioned the effectiveness of the preceding method for determining adatom heights above bulk atomic planes.[38] The best fit to these diffraction results has indeed been obtained considering two kinds of Sn adatoms with a height difference of 0.3 Å.

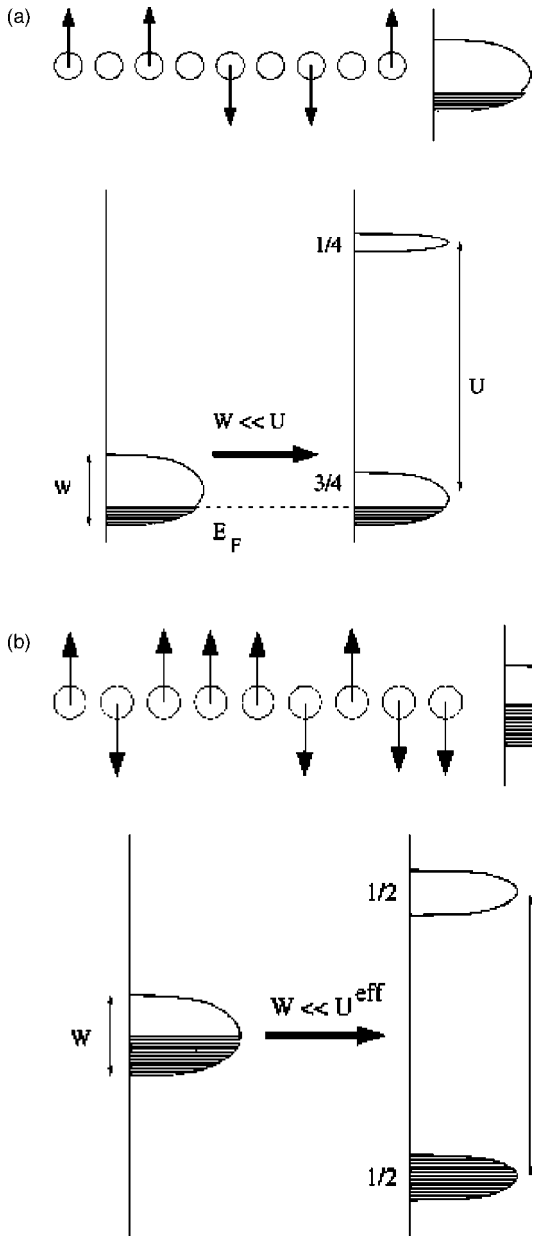

FIG. 7. Electron correlation effects in the Sn/Si(111)-α-$\sqrt{3}$ surface: (a) 3×3 case; (b) flat $\sqrt{3}\times\sqrt{3}$ case (see text). In (a) electron correlation effects change the LDA band at E_F, creating a new state at E_F+U_{eff} with 1/4th of the initial weight. The system remains metallic. If all the Sn adatoms were equivalent (b) the surface should be insulating.

V. THE γ PHASE

Figures 8(a),8(b) shows KRIPES spectra obtained on the γ phase (mosaic phase) for positive and negative polar angles along the directions $\overline{\Gamma K'}$ and $\overline{\Gamma M'}$ of the SBZ. A set

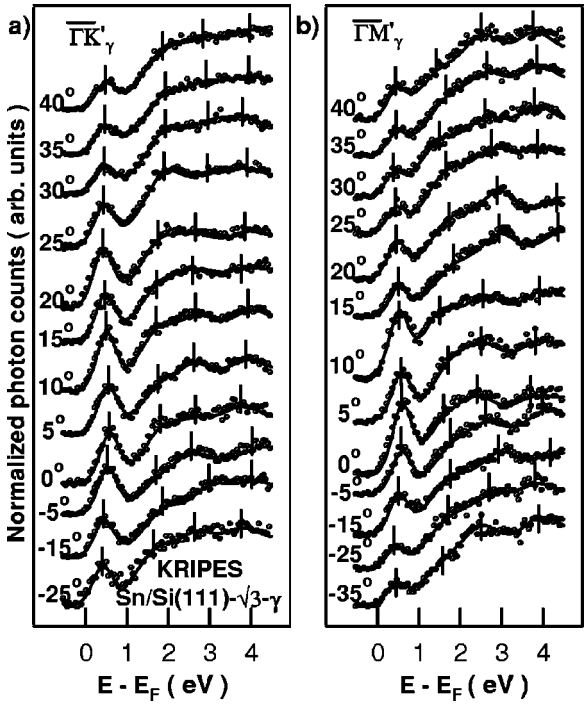

FIG. 8. KRIPES spectra of the γ-$\sqrt{3}$ (mosaic) reconstruction along the directions $\overline{\Gamma K'}$ (a) and $\overline{\Gamma M'}$ (b) of the SBZ for selected positive and negative angles of the incident electrons. The vertical bars represent the position of the maximum of each Gaussian.

of four Gaussians was required to fit these spectra in the range 0 to 5 eV above the Fermi level. The first state (U_1) is localized at 0.56 eV above E_F at $\overline{\Gamma}$ and the three others are at 1.71, 2.61, and 3.75 eV. These states disperse all over the surface Brillouin zone. In both directions $\overline{\Gamma K'}$ and $\overline{\Gamma M'}$, the intensity of U_1 is maximum at normal incidence (SBZ center) and decreases as the angle of incidence of the electrons increases towards the SBZ edges; conversely, the intensity of the upper states remains almost unchanged for all angles.

The band dispersion of these states are given in Fig. 9. The dispersion of U_1 tends to get closer to E_F near the SBZ edges; it reaches 0.38 eV at $\overline{K'}$, and its bandwidth is about 0.15 eV. Hence U_1 does not cross E_F and the surface is semiconducting. Previous ARUPS studies[16,39] have shown the presence of an occupied surface state at 0.1 eV below E_F. Therefore we can estimate the band gap to be around 0.5 eV. This semiconducting character has been confirmed by STS measurements, shown in Fig. 4(b). This curve represents an average of 47 measurements taken over the surface. On this spectrum, we observe the lack of current through the surface for applied voltage between 0 and 0.3 V indicating the presence of a gap around 0.3 eV.

The band dispersion of U_1 is in good agreement with the calculations presented above (see Fig. 2) for the $Si_{0.5}Sn_{0.5}/Si(111)$-$2\sqrt{3}\times\sqrt{3}$ surface, which represents the mosaic phase in a simplified way. Our DFT-LDA calculations show an energy gap of 0.25 eV between Sn-like filled states and Si-like empty states, in good agreement with the STM data, and a very narrow bandwidth of 0.1 eV for the

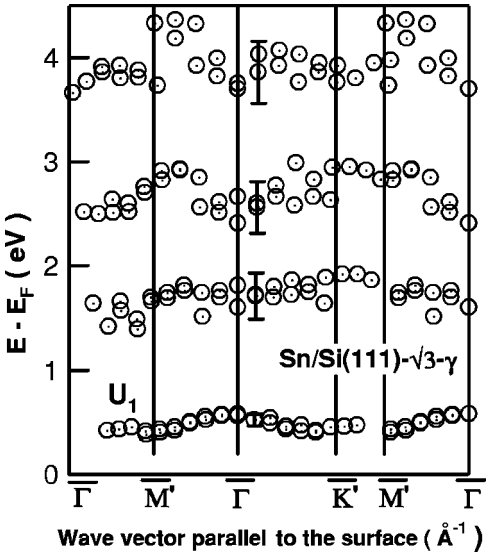

FIG. 9. Experimental band dispersion of the γ-$\sqrt{3}$ reconstruction. Electron energy is plotted against the wave vector parallel to the surface.

empty states. DFT-LDA calculations, which fail to describe the excited systems, are known to underestimate band gaps in insulators. Our KRIPES and LDA data are thus systematically shifted by ≈ 0.3 eV, suggesting that the energy gap is probably between 0.3 and 0.5 eV.

For the γ phase, we exposed the sample to 1 L of atomic hydrogen. Figure 10 shows the spectra obtained before (a) and after (b) exposition at $\overline{\Gamma}$ in the same conditions; (c) is the difference between the two previous spectra. Whereas the first state intensity has nearly decreased to zero, the higher energy states are not visible in the difference signal. Hence we can conclude that U_1 is a surface state and that the three upper states correspond to bulk states. Moreover, the shape of the dispersion of U_1 and its shift towards E_F as we get closer to the SBZ edges is characteristic, as for the α phase, of a surface state mainly derived from p_z-type orbital localized on the adatoms. This, in agreement with the STM and

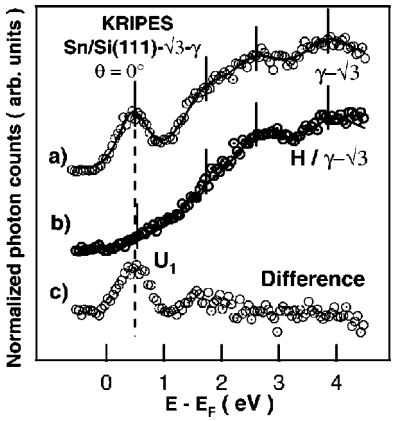

FIG. 10. (a) and (b) KRIPES spectra of the γ phase, respectively obtained before and after exposure of the sample at 1L of atomic hydrogen. (c) Subtraction (a)−(b).

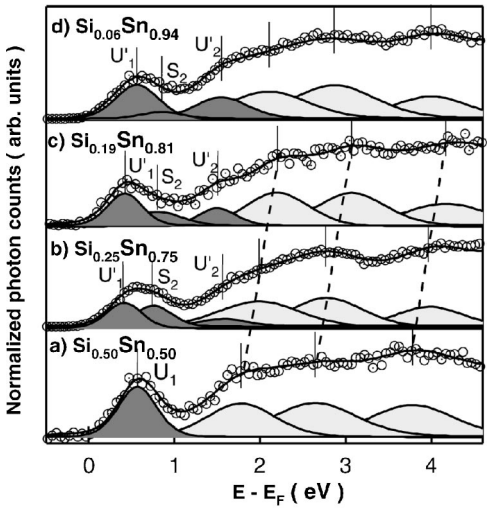

FIG. 11. KRIPES spectra obtained at normal incidence for (a) the γ phase, (b) the intermediate phase close to the mosaic phase (interm1), (c) an intermediate phase close to the α phase, and (d) the α phase.

LDA results, shows that U_1 is located primarily on Si adatoms.

VI. FROM THE MOSAIC TO THE α PHASE

Starting from the mosaic phase, we still have to explain how the surface evolves with increasing Sn coverage. Figure 11 shows four KRIPES spectra obtained at $\overline{\Gamma}$ on the following phases: (a) the mosaic phase, (b) a first intermediate phase interm$_1$ close to the mosaic; (c) a second intermediate phase interm$_2$ closer to the α phase, and (d) the α phase. The mosaic phase [Fig. 11(a)] presents a single surface state U_1 at 0.56 eV. According to the STM and LDA results, this state must be attributed to Si adatoms, as previously explained. The interm$_1$ phase [Fig. 11(b)] evidences three surface states U_1', S_2 and U_2'. These three states are also present on interm$_2$ [Fig. 11(c)]. However, the S_2 peak decreases when the Sn concentration increases while U_1' and U_2' become more intense. In conclusion, the intensity of S_2 follows the Si adatom concentration; S_2 is thus associated with Si adatoms. Therefore, S_2 and U_1 correspond to the same state. A similar argumentation confirms the attribution of U_1' and U_2' to Sn adatoms. This interpretation is confirmed by the behavior of the α phase [Fig. 11(d)] where these three peaks follow the same evolution. If the α phase was perfect, the S_2 peak would completely disappear. The weak residual intensity seen on Fig. 11(d) must be attributed to the few substitutional Si adatoms considered here as defects.

In order to identify theoretically the isolated Si-defect level [S_2 peak in Fig. 11(d)] we have also calculated a Si impurity in a Sn/Si-3×3 reconstruction. Without going into details, we only mention here that the Si-induced level is located around 0.2 eV above E_F, higher than U_1', in good agreement with the experimental data (taking into account the systematic shift between experimental and theoretical data mentioned above).

The first structures near E_F in Fig. 11 [U_1' and S_2 in Figs. 11(b)–11(d), or peak U_1 in Fig. 11(a)] have a global decreasing area when the amount of tin increases. This change in intensity is explained by the density of electrons in the bands. Although the adatom electronic density has not changed, their nature is different. In the case of the mosaic phase [Fig. 11(a)], two types of adatoms are present, Sn and Si, giving rise to two bands. As discussed above, the Sn-DB band is completely filled, while the Si-DB band is completely empty; therefore, the density of unoccupied states in the Si-band (U_1) is 1 electron per $\sqrt{3}$ unit cell. In the case of a perfect α phase [Fig. 11(d)], the state U_1' presents a total density of states of $3/4 \times 4 = 3$ electrons per 3×3 unit cell (see Sec. IV); this state is occupied by 1 electron (per 3×3 unit cell), leaving a density of unoccupied states of 2/3 of electron per $\sqrt{3}$ unit cell [see also Fig. 7(a)].[36]

The height of the U_1' peak on the α phase is accordingly lower than the one of U_1 on the γ phase. The density of electron attributed to each band is thus directly correlated to the peak areas, itself correlated to the stoichiometry of the surface. The area of the first two peaks for the two intermediate phases [Figs. 11(b),11(c)] is in between the α and mosaic ones. This stoichiometry can be determined by two different methods based on the individual component areas. In order to account for the finite surface state dispersion, an effective area has been calculated based on the peak intensity times the Gaussian FWHM for normal incidence artificially augmented by the overall bandwidth of the state. The first method consists in normalizing the area of the Si derived Gaussian (S_2) with a reference of known Si concentration similar to the spectrum obtained on the mosaic phase [we consider a perfect mosaic phase Fig. 11(a), where A_1, the U_1 Gaussian area corresponds to 50% of Si adatoms]. This method gives x, the concentration of Si adatoms, from which we deduce the Sn concentration $(1-x)$. In the second method, the Sn (U_1') and Si (S_2) Gaussian areas of a unique spectrum, respectively called A_{Sn} and A_{Si}, are normalized by their sum ($A_{\mathrm{Sn}}+A_{\mathrm{Si}}$). Before doing this calculation, each Gaussian area is normalized by the electron weight, i.e., 2/3 for Sn (U_1') and 1 for Si (S_2). Figure 12 compares the relative concentration of Si adatoms found for the three phases, α, interm2, and interm1 of Figs. 11(d), 11(c), 11(b), obtained by the two methods. The results obtained are very close to the ideal correspondance line. These calculations thus confirm our interpretation which attributes a weight of 2/3 of electrons on the U_1' component. On the basis of the relative weights of the components which have been attributed to Si and Sn adatoms, it is thus possible to deduce the relative concentrations of both species in the adatom layer from a single inverse photoemission spectrum.

We finally notice a shift towards the higher energies of the bulk states as the amount of tin is increased. This is attributed to a band bending effect.

VII. SUMMARY AND CONCLUSIONS

In this work, we have presented a detailed study of the electronic structure of Sn/Si(111)-($\sqrt{3}\times\sqrt{3}$)$R30°$ system at

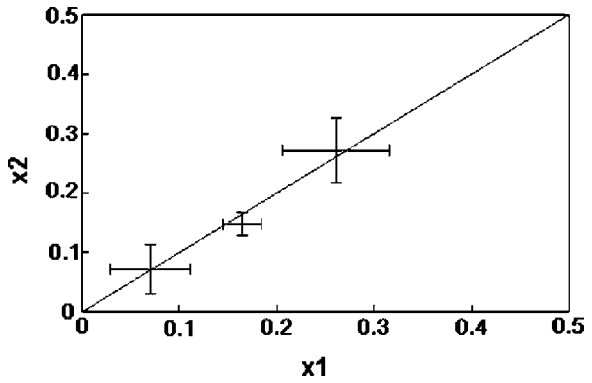

FIG. 12. Si concentration calculated from Figs. 11(b)–11(d) spectra with two different methods: x_1, first method and x_2, second method. See text for a description (Sec. IV) of the methods. The concentration x_2 has been obtained with a relative weight of 2/3 for the electronic densities of U_1' (Sn derived) with respect to S_2 (Si derived).

submonolayer coverages of Sn, with a particular emphasis on the unoccupied states. The electronic structure of the 2D solid solution $Si_xSn_{1-x}/Si(111)-(\sqrt{3}\times\sqrt{3})R30°$ at room temperature has been studied by global (KRIPES) and local (STM, STS) probes, as well as by DFT-LDA calculations. Depending on the Sn coverage between 1/6 and 1/3 ML, the adatom overlayer with a $(\sqrt{3}\times\sqrt{3})R30°$ symmetry shows contrasting electronic properties, including a semiconductor to metal transition. The $Si_{0.5}Sn_{0.5}/Si(111)$-$\sqrt{3}$ or mosaic phase has a single empty surface state localized at 0.56 eV above E_F at $\bar{\Gamma}$. With an overall bandwidth of ≈ 0.15 eV, this sp_z-type state localized on Si adatoms does not cross E_F: the mosaic phase is semiconducting, with a bandgap between 0.3 and 0.5 eV. This phase is characterized by a large corrugation of 0.75 Å with Sn adatoms higher than Si adatoms. In the Sn-rich limit $Si_xSn_{1-x}/Si(111)$-$\sqrt{3}$ with $x \leqslant 0.05$, we follow an empty state U_1' throughout most of the surface Brillouin zone (SBZ) except near the $\bar{K}$ point where it clearly crosses the Fermi level. A second, empty surface state U_2' is detected 1.67 eV above E_F. Once electron correlation effects are adequately taken into account, we explain our KRIPES results for the α phase as originating from an underlying (3×3) atomic geometry which is dynamically fluctuating at RT. These fluctuations are attributed to an incomplete softening of a surface phonon.[27]

ACKNOWLEDGMENTS

This work has been partially funded by the spanish CICYT under Project No. PB97-0028.

*Corresponding author: charrier@gpec.univ-mrs.fr

[1] T. Ichikawa, Surf. Sci. **140**, 37 (1984).
[2] D.T. Wang, N. Esser, M. Cardona, and J. Zegenhagen, Surf. Sci. **343**, 31 (1995).
[3] 1ML is defined as one metal atom for one Si atom of the first Si(111) layer which corresponds to a density of 7.84 10^{14} atoms/cm^2.
[4] J.M. Nicholls, B. Reihl, and J.E. Northrup, Phys. Rev. B **35**, 4137 (1987).
[5] C.A. Sebenne, *Surface Physics and Related Topics*, edited by Fu-Jia Yang *et al.* (World Scientific, Singapore, 1991), p. 259.
[6] J.M. Carpinelli, H.H. Weitering, and E. W. Plummer, Surf. Sci. **401**, L457 (1998).
[7] G. Le Lay, J. Phys. IV **7**, 115 (1997).
[8] J.E. Northrup and J. Neugebauer, Phys. Rev. B **52**, R17001 (1995).
[9] C. Törnevik, M. Göthelid, M. Hammar, U.O. Karlsson, N.G. Nilsson, S.A. Flodström, C. Wigren, and M. Östling, Surf. Sci. **314**, 179 (1994).
[10] J. Nogami, Sang-il Park, and C.F. Quate, J. Vac. Sci. Technol. A **7**, 1919 (1989).
[11] J.A. Kubby, Y.R. Wang, and W.J. Greene, Phys. Rev. Lett. **65**, 2165 (1990).
[12] E. Ganz, F. Xiiong, I.-S. Hwang, and J. Golovchenko, Phys. Rev. B **43**, 7316 (1991).
[13] C.J. Karlsson, E. Landemark, Y.-C. Chao, and R.I.G. Uhrberg, Phys. Rev. B **45**, 6321 (1992).
[14] X.F. Lin I. Chizhov, H.A. Mai, and R.F. Willis, Surf. Sci. **366**, 51 (1996).
[15] T. Kinoshita, S. Kono, and T. Sagawa, Phys. Rev. B **34**, 3011 (1986).
[16] T. Kinoshita, H. Ohta, Y. Enta, Y. Yaegashi, S. Suzuki, and S. Kono, J. Phys. Soc. Jpn. **56**, 4015 (1987).
[17] H. Ohta, T Kinoshita, Y. Yaegashi, S. Suzuki, and S. Kono, J. Phys. Soc. Jpn. **57**, 4432 (1988).
[18] M. Göthelid, M. Björkqvist, T.M. Grechk, G. Le Lay, and U.O. Karlsson, Phys. Rev. B **52**, R14352 (1995).
[19] J. Avila, A. Mascaraque, E.G. Michel, M.-C. Asensio, G. Le Lay, J. Ortega, R. Pérez, and F. Florés, Phys. Rev. Lett. **82**, 442 (1999).
[20] R.I.G. Uhrberg and T. Balasubramanian, Phys. Rev. Lett. **81**, 2108 (1998).
[21] J.M. Carpinelli, H.H. Weitering, M. Bartkowiak, R. Stumpf, and E.W. Plummer, Phys. Rev. Lett. **79**, 2859 (1997).
[22] O. Bunk *et al.*, Phys. Rev. Lett. **83**, 2226 (1999).
[23] J. Zhang, Ismail, P.J. Rous, A.P. Baddorf, and E.W. Plummer, Phys. Rev. B **60**, 2860 (1999).
[24] J. Ortega, R. Pérez, and F. Flores, J. Phys.: Condens. Matter **12**, L21 (2000).
[25] Slezák, P. Mutambo, and V. Cháb, Phys. Rev. B **60**, 13328 (1999).
[26] L. Ottaviano, M. Crivellari, L. Lozzi, and S. Santucci, Surf. Sci. **445**, L41 (2000).
[27] R. Pérez, J. Ortega, and F. Flores, Phys. Rev. Lett. **86**, 4891 (2001).
[28] S. Bouzidi, F. Coletti, J.-M. Debever, P.A. Thiry, P. Dumas, and Y. Chabal, Phys. Rev. B **45**, 1187 (1992).
[29] P.J. Timans, J. Appl. Phys. **74**, 6353 (1993).
[30] Remaining differences may be ascribed to the markedly different sizes of Sn and Si adatoms.
[31] A.A. Demkov, J. Ortega, O.F. Sankey, and M.P. Grumbach, Phys. Rev. B **52**, 1618 (1995); O.F. Sankey and D.J. Niklewski, *ibid.* **40**, 3979 (1989).

[32] J.-M. Themlin, I. Forbeaux, V. Langlais, H. Belkhir, and J.-M. Debever, Europhys. Lett. **39**, 61 (1997).
[33] J.M. Nicholls, P. Mårtensson, G.V. Hansson, and J.E. Northrup, Phys. Rev. B **32**, 1333 (1985).
[34] G. Le Lay, J. Janski, P.O. Nilsson, and U.O. Karlsson, Appl. Surf. Sci. **56/58**, 178 (1992).
[35] H.T. Anyele, C.L. Griffiths, A.A. Caffola, C.C. Matthai, and R.H. Williams, Appl. Surf. Sci. **123/124**, 480 (1998).
[36] A. Charrier, R. Pérez, F. Thibaudau, J.-M. Debever, J. Ortega, F. Flores, and J.-M. Themlin, J. Phys. Condens. Matter **13**, L521 (2001).
[37] K.M. Conway *et al.*, Surf. Sci. **215**, 555 (1989).
[38] T. Yamanaka and S. Ino, Phys. Rev. B **61**, R5074 (2000).
[39] C. Karlsson, Y.-C. Chao, E. Landemark, and R.I.G. Uhrberg (unpublished).